# Molecular and morphological evidence for a new species of the genus *Typhlomys* (Rodentia: Platacanthomyidae)

**DEAR EDITOR,**

In this study, we reassessed the taxonomic position of *Typhlomys* (Rodentia: Platacanthomyidae) from Huangshan, Anhui, China, based on morphological and molecular evidence. Results suggested that *Typhlomys* is comprised of up to six species, including four currently recognized species (*Typhlomys cinereus*, *T. chapensis*, *T. daloushanensis*, and *T. nanus*), one unconfirmed candidate species, and one new species (*Typhlomys huangshanensis* **sp. nov.**). Morphological analyses further supported the designation of the Huangshan specimens found at mid-elevations in the southern Huangshan Mountains (600 m to 1 200 m a.s.l.) as a new species.

The family Platacanthomyidae is comprised of two extant genera, *Platacanthomys* and *Typhlomys* (Musser & Carleton, 2005). Molecular phylogenetic findings support Platacanthomyidae as a unique lineage and sister to all other Muroidea families, although their external morphology is similar to dormice of the family Gliridae and their molar structure is similar to *Gymnuromys* from Madagascar (Abramov et al., 2014; Jansa et al., 2009; Musser and Carleton, 2005).

The genus *Typhlomys* (Milne-Edwards, 1877), which means "blind mouse" (Jansa et al., 2009), possesses small shrew-like eyes and is the lesser-known member of Platacanthomyidae. These animals have a long hairy tail, long vibrissae, and prominent ears, with the tip of their tails covered in a tuft of long white hair (Hong, 1982). Their long vibrissae are a tactile aid in the capture of prey (Anjum et al., 2006), and their short limbs exhibit scansorial and fossorial advantage in terms of leverage (Rubin & Lanyon, 1984). Such morphological adaptations suggest an arboreal and burrowing lifestyle (Cui et al., 2020; Smith, 2008). As an arboreal animal with vestigial eyes, these rodents have developed a form of echolocation for orientation and navigation in complex environments without visual assistance (Panyutina et al., 2017). Although eye degradation (Cheng et al., 2017) is a feature present in other mammals, such as moles (Carmona et al., 2008), it is usually associated with fossoriality and is uncommon among scansorial/arboreal species; *Typhlomys* is the only currently known taxon.

Despite the unique morphology and life history of this genus, the exact species composition of *Typhlomys* is still unclear (Jansa et al., 2009). In the original taxonomic description based on pelage, external measurements, and skull morphometrics, *Typhlomys* contained five subspecies, including *Typhlomys cinereus cinereus*, *T. c. chapensis*, *T. c. daloushanensis*, *T. c. guangxiensis*, and *T. c. jingdongensis* (Wang et al., 1996). Subsequently, Abramov et al. (2014) supported the specific status of *T. c. chapensis* given the significant molecular and skull morphology differences between this subspecies and nominal *T. c. cinereus*. Recent molecular phylogenetic studies confirmed the monophyly of *Typhlomys* and suggested that it is composed of at least five species based on genetic evidence of multiple loci and skull morphology and morphometrics (Cheng et al., 2017). The research of Cheng et al. (2017) determined the species level recognition of *T. cinereus*, *T. daloushanensis*, and *T. chapensis*, described a new species (*T. nanus*), and identified a putative new species.

*Typhlomys* is mainly distributed in montane regions of southern China and northwestern Vietnam (Abramov et al., 2014; Cong et al., 2013). As a mid-high elevation inhabitant (340–2 300 m a.s.l.), the distribution of *Typhlomys* is strongly related to complex geographical regions (Abramov et al., 2012). For example, in southwest China, the extremely complex topography and well-developed river systems in the

Hengduan Mountain region have led to the allopatric divergence of species within the genus *Typhlomys* (Chen et al., 2017; Fjeldså et al., 2012; Liu et al., 2012) and may have led to the differentiation of two different genetic populations (*T. nanus* and *T. chapensis*, Cheng et al., 2017). In southeast China, there are similar river valley systems (Song et al., 2017), but only one species (*T. cinereus*) has been discovered to date (Cong et al., 2013; Wang, 1990; Wang et al., 1996). Thus, to some extent, the species diversity of *Typhlomys* may be underestimated.

In the present study, we integrated molecular and morphometric approaches to describe a new species from the Huangshan and Qingliangfeng mountains in Anhui Province, China.

Blind mouse specimens were collected from the Huangshan and Qingliangfeng mountains (Anhui Province, China) and consisted of four adult males and six adult females. Tissue samples were extracted, amplified, and sequenced for the cytochrome *b* (cyt *b* ) gene (1 070 bp), interphotoreceptor retinoid-binding protein (*IRBP* (1 052 bp)) gene, and growth hormone receptor (*GHR* (774 bp)). All DNA sequences generated are available in GenBank (Supplementary Table S1). Uncorrected pairwise genetic distances of the cyt *b* gene were computed using the APE R package (Paradis et al., 2004). Bayesian phylogenetic analyses were conducted with MrBayes v3.2.2, including each nuclear gene, cyt *b* gene, and concatenated mitochondrial and nuclear datasets (Ronquist et al., 2012). The Poisson tree processes (PTP) model (Zhang et al., 2013) and BPP v3.4 (Yang & Rannala, 2010) were run to infer putative species boundaries (see Supplementary Materials and Methods). Divergence times among putative species were estimated with BEAST v1.7.4 based on the concatenated gene (Bouckaert et al., 2014). Specimens collected for morphometric analyses, combined with detailed skull data from Cheng et al. (2017), included two *T. cinereus*, 29 *T. daloushanensis*, 21 *T. chapensis*, three *T. nanus*, and nine *T.* sp. 1 specimens. Morphometric data were taken using digital calipers to the nearest 0.01 mm (Table 1), and following the measurements described in Cheng et al. (2017) (Supplementary Materials and Methods). The skull of voucher specimen AE1902HS04 was broken in transit, so its associated morphometric data are missing from this study. Principal component analysis (PCA) and canonical discriminant function analysis (DFA) were used to compare genetically delineated groups within the genus *Typhlomys* (Supplementary Materials and Methods).

The combined mitochondrial-nuclear gene and nuclear gene phylogenetic reconstructions recovered similar topologies as Cheng et al. (2017) (Figure 1A-b, c, d), and the monophyly of these lineages was strongly supported (Bayesian posterior probability (PP) ≥0.99). Among them, one clade was comprised of *T. chapensis* (Clade A) and *T. nanus* (Clade B); the other clades (C-F) corresponded with *T. cinereus*, *T. daloushanensis*, previously identified cryptic species (*T.* sp. 2), and newly identified species (*T.* sp. 1), respectively. Overall, the relationship between *T. cinereus* (clade E) and *T.* sp. 1

(clade F) was strongly supported as sister species (PP≥0.99). In the mitochondrial cyt *b* gene tree (Figure 1A-a), the phylogenetic tree still showed the same topological structure with an additional *T. cinereus* from Guangdong (Lv et al., 2016).

The cyt *b* uncorrected genetic distances among different species ranged from 11.3% to 19.2% (Supplementary Table S4). Considering that species-level divergence in different mammal groups ranges from 2% and 11% (Baker & Bradley, 2006), the different lineages of *Typhlomys* (A–F, Figure 1A-a) might represent distinct species. Among them, the genetic distance between *T.* sp. 1 and *T. cinereus* was 14.2%–14.7% (Supplementary Table S4), indicating species-level divergence. We also observed a single triplet insertion (*T. chapensis*, *T. nanus*) and single triplet deletion (*T. cinereus*, *T.* sp. 1, *T.* sp. 2) in the IRBP sequences.

The topology of the species tree resembled the concatenated gene tree, and all relationships were strongly supported (Figure 1B). The time to the most recent common ancestor (MRCA) of *Typhlomys* was estimated to be 16.94 million years ago (Ma) (95% CI=9.70–26.31). Furthermore, the six putative species diverged between 6.90 and 11.49 Ma, and *T.* sp. 1 and *T. cinereus* diverged about 7.72 Ma (95%CI=4.41–11.40).

The Poisson tree processes (PTP) model for species delimitation recognized eight putative species (Figure 1B-a), and the split results supported the specific status of *T. cinereus* and *T.* sp. 1, with species partition support of 0.98 and 0.95, respectively (Figure 1B-a). Based on the results of Cheng et al. (2017), we used BPP to test a six species scenario (Figure 1B-b). The results supported the validity of all six species with high posterior probabilities (PP≥0.99, Supplementary Table S5) and the specific status of *T.* sp. 1 (PP≥0.99).

A summary of the descriptive morphometric variables is given in Supplementary Table S2. Based on principal component analysis of the 11 craniodental measurements, the eigenvalues of two factors exceeded 1.0. The first principal component (PC1) explained 63.52% of total variation, with an eigenvalue of 6.987, which was dominated by ZMW, GLS, LUIM, CBL, BL, $M^1$–$M^1$, LNM–FLM, HCV, and UML (descriptions of all morphometric acronyms can be found in Table 1). The second principal component (PC2) explained 14.66% of total variation, with an eigenvalue of 1.613, which was mainly related to IOB and BCH. The two factors diverged along the first principal component, reflecting differences in overall cranial size. The principal component biplot (Figure 1C) showed that the *T. daloushanensis* specimens were mostly clustered in the positive region of PC1 and that *T. chapensis* occupied the positive region of PC2, consistent with the results of Cheng et al. (2017). The other three groups, *T. nanus*, *T. cinereus*, and *T.* sp. 1, were all in the negative field of PC1 and PC2 but were completely separated. Among them, males of *T.* sp. 1 had longer and wider skulls overall than females.

Discriminant function analysis of the same variables corr-

ectly classified 100% of morphometric distinctions (Figure 1C). Canonical axes 1, 2, and 3 explained 59.7%, 34.9%, and 4.4% of total variation, respectively. The first canonical axis (CAN1) mainly included ZMW, LNM–FLM, HCV, and UML. The second axis, based on standardized canonical coefficients (CAN2), consisted of GLS, CBL, and $M^1$–$M^1$.

Phylogenetic analysis showed a significant divergence between *T.* sp. 1 and *T. cinereus* ( Figure 1A). The genetic distances between *T.* sp. 1 and its nearest species (*T. cinereus*) was greater than 14% (Supplementary Table S4), reflecting species-level divergence (Bradley & Baker, 2006). These results indicate that *T.* sp. 1 is distinct from all recognized species and support its recognition at the species level. PTP and BPP analyses recognized eight and six putative species, respectively, and supported *T.* sp. 1 and *T. cinereus* as separate species (Figure 1B). Therefore, *T.* sp. 1 should be treated as a new species, and as sister species to *T. cinereus.* The divergence of *T.* sp. 1 and *T. cinereus* occurred at least as far back as the Middle Pliocene to Late Miocene. In addition, our research indicated that *Typhlomys* diversification began between the Middle and Late Miocene (Figure 1B), which may be related to the rapid uplift of the Qinghai-Tibetan Plateau and repeated paleoclimatic changes (Cheng et al., 2019; Liu et al., 2017; Wan et al.; 2018). Similar

**Table 1 External and cranial morphological measurements (mm) of *Typhlomys***

| Variable | *T. cinereus*(n=2) | *T. daloushanensis*(n=29) | *T. chapensis*(n=21) | *T. nanus*(n=3) | *T.* sp. 1(n=9) |
|---|---|---|---|---|---|
| TL | 99.00±4.24 | 116.80±5.35 | 106.00±1.45 | 102.00±4.58 | 98.87±5.11 |
| | 96.00–102.00 | 105.00–129.00 | 80.00–126.00 | 97.00–106.00 | 91.00–107.00 |
| HB | 73.50±3.54 | 86.05±6.55 | 77.59±10.87 | 70.00±4.58 | 77.49±4.69 |
| | 71.00–76.00 | 72.00–105.00 | 61.00–115.00 | 65.00–74.00 | 70.00–86.54 |
| HL | 18.80±1.13 | 22.93±1.33 | 21.43±1.21 | 19.67±0.58 | 19.08±1.21 |
| | 18.00–19.60 | 21.00–26.00 | 19.00–24.00 | 19.00–20.00 | 17.00–21.00 |
| EL | | 16.03±1.41 | 17.56±1.26 | 17.00±0 | 13.17±1.78 |
| | | 13.50–21.00 | 14.00–20.00 | 17.00–17.00 | 11.00–16.00 |
| WG | | 22.98±3.68 | 16.93±3.58 | 10.47±2.39 | 15.33±2.50 |
| | | 15.40–31.00 | 7.70–22.60 | 8.80–13.20 | 12.03–20.40 |
| GLS | 22.20±1.11 | 24.90±1.24 | 23.38±1.17 | 21.55±1.08 | 22.10±0.95 |
| | 21.40–23.00 | 23.74–26.33 | 21.65–24.82 | 20.93–22.16 | 20.60–23.43 |
| CBL | 20.15±1.01 | 22.74±1.14 | 21.26±1.06 | 19.83±0.99 | 20.48±0.88 |
| | 19.70–20.60 | 21.39–24.45 | 20.05–22.16 | 19.76–19.89 | 19.21–21.75 |
| BL | 18.25±0.91 | 20.81±1.04 | 19.46±0.97 | 17.93±0.90 | 18.71±0.27 |
| | 17.70–18.80 | 19.50–22.51 | 18.37–20.50 | 17.54–18.31 | 18.28–18.99 |
| IOB | 4.80±0.24 | 4.99±0.25 | 5.27±0.26 | 4.79±0.24 | 4.75±0.06 |
| | 4.70–4.90 | 4.55–5.43 | 5.00–5.60 | 4.77–4.81 | 4.67–4.83 |
| BCH | 7.70±0.39 | 7.82±0.39 | 7.94±0.40 | 7.11±0.36 | 7.52±0.24 |
| | 7.50–7.90 | 7.23–8.91 | 7.35–8.46 | 7.04–7.18 | 7.11–7.88 |
| ZMW | 11.80±0.59 | 13.86±0.69 | 12.64±0.63 | 11.55±0.58 | 12.48±0.18 |
| | 11.40–12.20 | 13.08–15.05 | 12.00–13.39 | 11.35–11.74 | 12.18–12.69 |
| UML | 3.30±0.17 | 3.81±0.19 | 3.61±0.18 | 3.31±0.17 | 3.74±0.16 |
| | 3.20–3.40 | 3.57–4.05 | 3.46–3.85 | 3.13–3.49 | 3.56–4.05 |
| LUIM | 10.70±0.54 | 12.00±0.60 | 11.34±0.57 | 10.13±0.51 | 10.89±0.24 |
| | 10.40–11.00 | 11.42–12.65 | 10.69–12.02 | 10.08–10.17 | 10.61–11.34 |
| $M^1$–$M^1$ | 5.05±0.25 | 5.57±0.28 | 5.31±0.27 | 4.91±0.25 | 4.90±0.11 |
| | 5.00–5.10 | 5.31–5.83 | 5.05–5.52 | 4.80–5.01 | 4.72–5.03 |
| HCV | 4.05±0.20 | 4.59±0.23 | 3.99±0.20 | 3.96±0.20 | 4.14±0.25 |
| | 3.80–4.30 | 4.20–5.06 | 3.60–4.37 | 3.81–4.11 | 3.77–4.52 |
| LNM–FLM | 5.95±0.30 | 6.76±0.34 | 6.37±0.32 | 5.83±0.29 | 6.03±0.18 |
| | 5.60–6.30 | 4.96–7.35 | 6.05–6.57 | 5.79–5.86 | 5.75–6.33 |

TL: Tail length; HB: Head and body length; HL: Hind foot length; EL: Ear length; WG: Weight; GLS: Greatest length of skull; CBL: Condylobasal length; BL: Basal length; IOB: Interorbital breadth; BCH: Braincase height; ZMW: Zygomatic width; UML: Upper molar row length; LUIM: Length between upper incisor and molar; $M^1$-$M^1$: Crown breadth of $1^{st}$ upper molars; HCV: Height of coronoid valley; LNM-FLM: Length between backmost notch point of mandibular and front of lower molars. External and cranial morphological measurements of cheek teeth of above species were obtained from Cheng et al. (2017), except for *T.* sp. 1.

(a) *Cytb*  (b) *GHR*  (c) *IRBP*  (d) mtDNA+nDNA

(a) PTP  (b) BPP

(a) PCA  (b) DFA
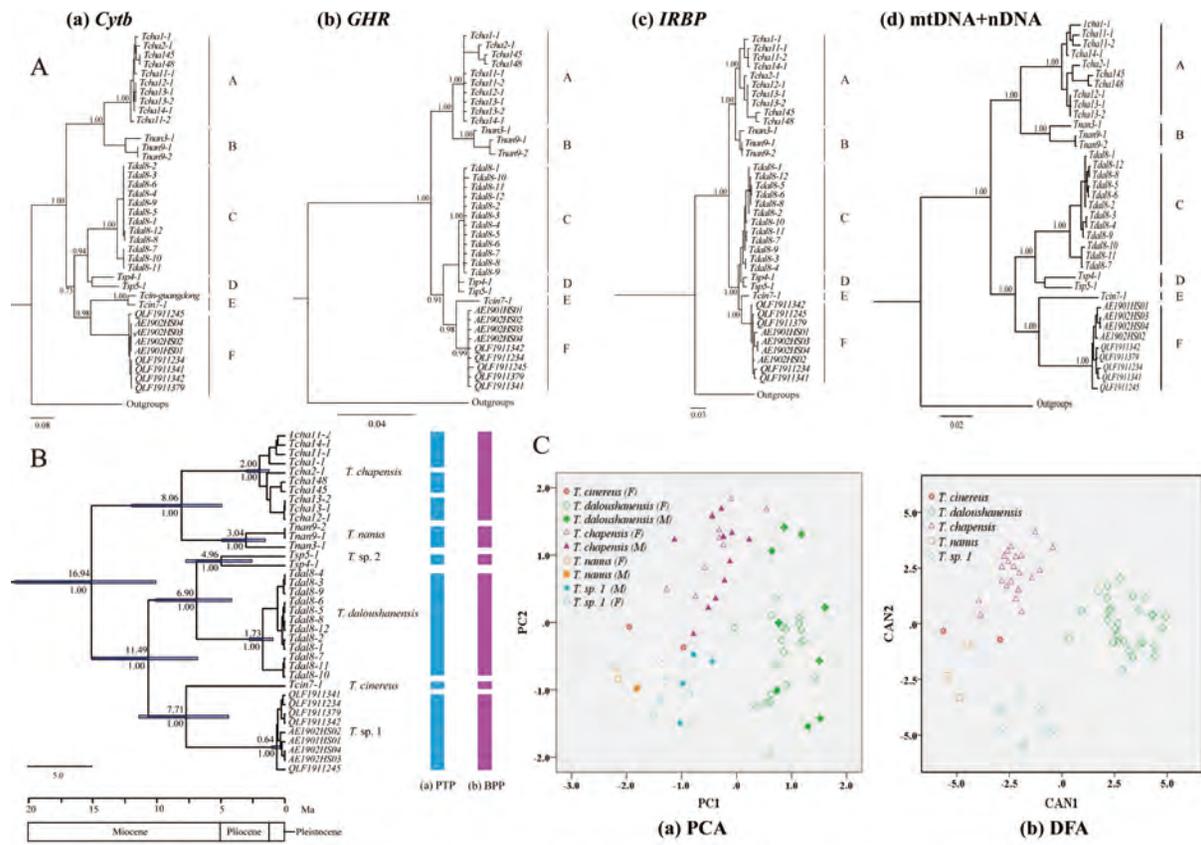
(a) *T.* sp. 1
(*T. huangshanensis* sp. nov.)

(b) *T. nanus*  (c) *T. chapensis*  (d) *T. daloushanensis*  (e) *T. cinereus*
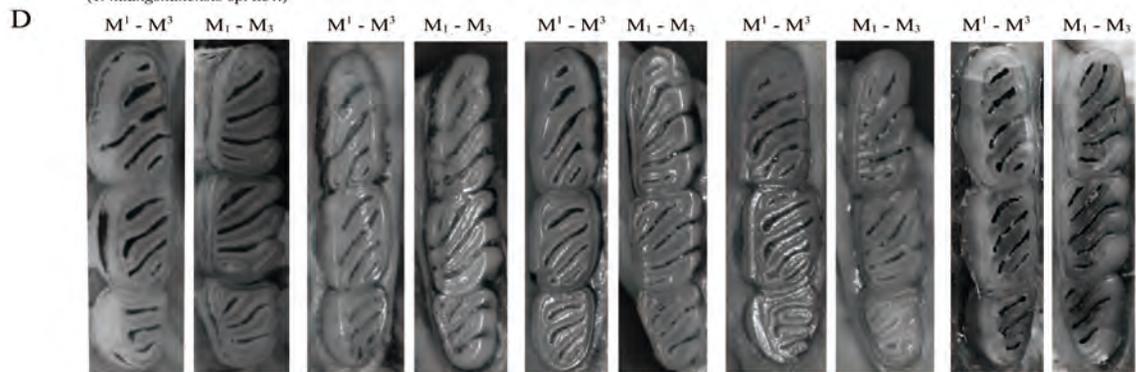
$M^1 - M^3$  $M_1 - M_3$

**Figure 1 Phylogenetic tree, species delimitation, and principal component and discriminant function analysis of *Typhlomys*, with skulls and dorsal views of *Typhlomys huangshanensis* sp. nov. and molar comparisons of five species**

A: Bayesian phylogenetic trees derived from cyt *b* (a), *GHR* (b), *IRBP* (c), and concatenated nuclear and mitochondrial (d) sequences. Letters near branches correspond to different species: A: *T. chapensis*; B: *T. nanus*; C: *T. daloushanensis*; D: *T.* sp. 2; E: *T. cinereus*; F: *T.* sp. 1. B: Species delimitation using PTP (a) and BPP (b), and nuclear gene species trees reconstructed with *BEAST. Node numbers are posterior probabilities (upper) and median ages of divergence times (lower). C: Results of principal component analysis (PCA) (a) and discriminant function analysis (DFA) (b). D: Right upper and lower molars of *Typhlomys huangshanensis* **sp. nov.** (holotype, AE1902HS03) (a), *T. nanus* (KIZ 033585) (b), *T. chapensis* (KIZ 033593) (c), *T. daloushanensis* (KIZ 033556) (d), and *T. cinereus* (USNM 141495) (e). E: Ventral, dorsal, and lateral views of skull and lingual side of mandibles of *Typhlomys huangshanensis* **sp. nov.** a: Female (paratype, AE1901HS01); b: male (holotype, AE1902HS03). F: Dorsal views of skin of holotype (upper) and paratype (lower). Except for *Typhlomys huangshanensis* **sp. nov.**, cheek teeth figures of above species were obtained from Cheng et al. (2017).

processes have been suggested for the diversification of *Uropsilus* ( Wan et al., 2013), *Perognathus* ( Riddle et al., 2014), and *Apodemus* (Michaux et al., 2002).

The distribution of the six different species showed a distinct geographic pattern (Supplementary Figure S1), which could be partly due to the complex topography, developed river systems, and low dispersal ability of the animals (Cheng et al., 2017; Fu & Zeng, 2008; Hinckley et al., 2020; Zhou et al., 2012). On the other hand, in southeast China, scattered mountain ranges with high elevations, such as the Wuyi and Huangshan mountains, form potential sky islands and show allopatry in isolated areas (McCormack et al., 2009). These mountains span a wide altitudinal range that helps to buffer changes in climate and has provided continuously suitable habitats for *Typhlomys* since the early Late Miocene (He et al., 2019; Wu et al., 2013). The complex topography of these mountains may facilitate allopatric speciation over long evolutionary timescales by physical isolation, eventually resulting in the appearance of narrowly distributed endemic species.

With respect to the previous taxonomy of *Typhlomys*, dental formulas and skulls are used as keys for species diagnosis. Measurements for *Typhlomys* are provided in Table 1 and photographs of the skulls and teeth are provided in Figure 1D, E. Based on the PCA and DFA results, *T.* sp. 1 did not aggregate with other species.

Based on the above measurements, *T.* sp. 1 has a shorter and narrower skull (GLS=20.60–23.43, ZMW=12.18–12.69, $M^1$-$M^1$=4.72–5.03) than *T. daloushanensis* (GLS=23.74–26.33, ZMW=13.08–15.05, $M^1$–$M^1$=5.31–5.83), although both have flattened braincases. Regarding the upper molars, the anterofossette on $M^1$ of *T. daloushanensis* is much wider than that of *T*. sp. 1, and the anterofossette is present on M², whereas it is absent in *T.* sp. 1. Furthermore, *T. daloushanensis* has yellowish-white hair on its hind feet, which differs from the black pelage of *T.* sp. 1.

In addition, *T.* sp. 1 has a narrower interorbital breadth (IOB=4.67–4.83) than *T. chapensis* (IOB=5.00–5.60). The latter has a distinct dome-shaped skull, which is flattened in *T.* sp. 1. The mesofossettid on $M_1$ of *T. chapensis* is usually open on the buccal side but closed in *T*. sp. 1. The dorsal pelage is yellowish gray in *T. chapensis*, but brownish gray in *T.* sp. 1.

*Typhlomys* sp. 1 has a wider zygomatic breadth (ZMW=12.18–12.69) than *T. nanus* (ZMW=11.35–11.74). The

former also has a flattened braincase, whereas *T. nanus* has a dome-shaped braincase. *Typhlomys* sp. 1 has a posterofossettid on $M_1$, which is absent in *T. nanus*. The mesofossettid on $M_1$ is open in *T. nanus* but closed in *T.* sp. 1.

*Typhlomys* sp. 1 (GLS=20.60–23.43) and *T. cinereus* (GLS=21.40–23.00) have a similar skull size and dome-shaped braincase, but *T.* sp. 1 has a longer upper molar (UML=3.56–4.05) than *T. cinereus* (UML=3.20– 3.40). The anterofossettes on $M^1$ in *T.* sp. 1 are narrower than those in *T. cinereus*. Furthermore, *T.* sp. 1 has inconspicuous $M_2$ anterofossettids, which are wide and very well developed in *T. cinereus*.

## Taxonomic account

*Typhlomys huangshanensis* Hu & Zhang, **sp. nov.**

**Holotype**: AE1902HS03. Dried skin (Figure 1F) and cleaned skull of an adult male, collected on 12 February 2019 by Lie Yu.

**Type locality**: Monkey Valley of Huangshan Mountains (N30.119, E118.306, 710 m a.s.l.), Tangkou Township, Huangshan City, Anhui Province, China. The specimen was deposited in the Biological Museum of Anhui University, Anhui, China.

**Paratypes**: AE1901HS01 (Figure 1F) and AE1901HS02, two adult females, collected on 10 January 2019 by Lie Yu from Monkey Valley, Tangkou Township, Huangshan City, Anhui Province, China (N30.119, E118.306, 710 m a.s.l.). QLF1911245 and QLF1911341, two adult males, collected on 20 November 2019 by Zhongzheng Chen from Qingliangfeng Mountains, Xuancheng City, Anhui Province, China (N30.130, E118.845, 1 303 m a.s.l.; N30.138, E118.825, 1 040 m a.s.l.). QLF1911244, QLF1911234, QLF1911379, and QLF1911342, collected on 25 November 2019 by Zhong-Zheng Chen from Qingliangfeng Mountains, Xuancheng City, Anhui Province, China (N30.130, E118.844, 1 228 m a.s.l.). The above specimens were prepared as dried skins with cleaned skulls.

Measurements of holotype (mm): AE1901HS03. Weight= 20.40 g; head and body length=86.54; tail length=98.30; hind foot length=18.13; ear length=11.46; greatest length of skull= 21.05; condylobasal length=19.85; basal length=18.34; interorbital breadth=4.83; braincase height=7.81; zygomatic width=12.97; length between upper incisor and molar=10.98; upper molar row length=4.05; crown breadth of 1st upper molars=5.10; height of coronoid valley=5.01; length between

backmost notch point of mandibular and front of lower molars=6.22.

**Diagnosis:** The new species can be distinguished by a flattened braincase rather than the domed braincases of *T. nanus* and *T. chapensis*. It has a shorter skull than *T. daloushanensis* and a narrower interorbital breadth than *T. chapensis*. Its hind feet are covered with black hair, differing from the yellowish-white hair of *T. daloushanensis.* It has a longer upper molar than *T. cinereus.* In the new species, the anterofossettes on $M^1$ are narrower than those in *T. cinereus*, and the anterofossettid of $M_2$ is missing or inconspicuous.

**Description**: A slightly smaller species in the genus *Typhlomys* (HB=77.49± 4.69; GLS=22.10±0.95). The dorsal and ventral pelage have two distinct colors: the dorsal pelage is brownish gray, while the ventral pelage is gray and covered with creamy white hair. The dorsal surfaces of the hind feet are covered with black hair. The braincase is flattened, and its height is relatively low. The palatal holes are relatively developed and usually have 2–3 columns. Upper molars are wide; with $M^2$ anterofossettes missing; $M^3$ lacks the anterofossette and posterofossette. The $M_1$ anterofossettid is shorter than the mesofossettid, which is closed, and the metalophid is long and developed, with an anterior extra ridge present, which merges with the metalophid at the anterolophid. The posterofossettid is complete. The $M_2$ anterofossettid is almost inconspicuous, and the posterofossettid is absent on $M_3$.

**Ecology and habitat**: The specimens were captured from a mixed evergreen and deciduous broad-leaved forest belt. Other sympatric small mammals included *Apodemus agrarius*, *Apodemus draco*, *Callosciurus erythraeus*, *Micromys minutus,* and *Crocidura anhuiensis* (Wang, 1990; Zhang et al., 2019).

**Distribution**: *Typhlomys huangshanensis* **sp. nov.** is currently known from the Huangshan and Qingliangfeng mountains, Anhui Province, China. The known elevational range is 710–1 303 m a.s.l.. It might occur in other mountain areas in southern Anhui and western Zhejiang.

**Etymology**: The specific name refers to its type locality, i.e., Huangshan Mountains, Anhui Province, China. We suggest the English common name as "Huangshan blind mouse" and the Chinese common name as "黄山猪尾鼠".

### Key to species of *Typhlomys*

1a) Dome-shaped braincase, narrow molars, mesofossettid on $M_1$ open buccally....................................................................2
1b) Flattened braincase, wide molars, mesofossettid on $M_1$ closed…………….......................................................................3
2a) GLS>21.6 mm, LUIM>10.6 mm, IOB>5.0 mm, posterofossettid and posterolophid on $M_1$ present........*T. chapensis*
2b) GLS<22.2 mm, LUIM<10.2 mm, IOB<4.9 mm, posterofossettid on $M_1$ absent.................................................*T. nanus*
3a) GLS<23.5 mm, BL< 19.0 mm, LUIM<11.4 mm, dorsal surface of hind feet black.....................................................4
3b) GLS>23.7 mm, BL>19.5 mm, LUIM>11.4 mm, dorsal surface of hind feet yellowish white............*T. daloushanensis*

4a) UML<3.4 mm, anterofossette on $M^1$ relatively wide, anterofossettid on $M_2$ wide and very well developed........
.............................................................................*T. cinereus*
4b) UML>3.5 mm, anterofossette on $M^1$ narrow, anterofossettid on $M_2$ absent or almost disappeared........................
.................................................................*T. huangshanensis*

### Comments

For a long time, only a single species of the genus *Typhlomys* (*T. cinereus*) was described in southeastern China (Wang, 1990; Wang et al., 1996). In the present study, the molecular and morphological results clearly suggest that *Typhlomys huangshanensis* **sp. nov.** is an new species and differs from all other congeners within the genus. This takes the number of species within the genus *Typhlomys* to six. All specimens of the new species were obtained from the Huangshan and Qingliangfeng mountain areas, but we believe the new species likely has a larger distribution, including at least southern Anhui and western Zhejiang. We do not yet know whether *Typhlomys huangshanensis* **sp. nov.** is sympatric with *T. cinereus* or not, and we do not know the distribution boundary between them. Based on the reported description of the distribution of *Typhlomys* sp. in southeastern China (southern Anhui, Zhejiang, and Fujian, Cheng et al., 2017; Wang, 1990; Wang et al., 1996), the distribution of *Typhlomys huangshanensis* **sp. nov.** is worthy of further investigation.

### NOMENCLATURAL ACTS REGISTRATION

The electronic version of this article in portable document format represents a published work according to the International Commission on Zoological Nomenclature (ICZN), and hence the new names contained in the electronic version are effectively published under that Code from the electronic edition alone (see Articles 8.5–8.6 of the Code). This published work and the nomenclatural acts it contains have been registered in ZooBank, the online registration system for the ICZN. The ZooBank LSIDs (Life Science Identifiers) can be resolved and the associated information can be viewed through any standard web browser by appending the LSID to the prefixhttp://zoobank.org/.
Publication LSID:
urn:lsid:zoobank.org:pub: 5B150064-C727-4A77-BB5C-6D6FE 3509C7D.
*Typhlomys huangshanensis* LSID:
urn:lsid:zoobank.org:act: 778976E1-1 556-4BE9-939E-EFF85B DF113F.

### SCIENTIFIC FIELD SURVEY PERMISSION INFORMATION

Permission for field surveys in Huangshan City, Anhui Province was granted by the Management Office of Huangshan Scenic Area.

### SUPPLEMENTARY DATA

Supplementary data to this article can be found online.

## COMPETING INTERESTS

The authors declare that they have no competing interests.

## AUTHORS' CONTRIBUTIONS

B.W.Z. conceived and designed the study. T.L.H. performed the experiments, analyzed the data, and prepared the manuscript. F.C. provided and helped analyze the data. Z.X., Z.Z.C., L.Y., Q.B., C.L.L., and T.P. collected materials. All authors read and approved the final version of the manuscript.

Ting-Li Hu[1,#], Feng Cheng[2,#], Zhen Xu[1],
Zhong-Zheng Chen[3,*], Lei Yu[1,5], Qian Ban[1], Chun-Lin Li[4],
Tao Pan[1], Bao-Wei Zhang[1,5,*]

[1] *School of Life Sciences*, *Anhui University*, *Hefei*, *Anhui* 230601, *China*

[2] *Unit of Evolutionary Biology/Systematic Zoology*, *Institute of Biology and Biochemistry*, *University Potsdam*, *Potsdam*, *Brandenburg* 14476, *Germany*

[3] *Collaborative Innovation Center of Recovery and Reconstruction of Degraded Ecosystem in Wanjiang Basin Co-founded by Anhui Province and Ministry of Education*, *School of Ecology and Environment*, *Anhui Normal University*, *Wuhu*, *Anhui* 241000, *China*

[4] *School of Resources and Environmental Engineering*, *Anhui University*, *Hefei*, *Anhui* 230601, *China*

[5] *International Collaborative Research Center for Huangshan Biodiversity and Tibetan Macaque Behavioral Ecology*, *Hefei*, *Anhui* 230601, *China*

[#]Authors contributed equally to this work
*Corresponding authors, E-mail: zhangbw@ahu.edu.cn; zhongzheng112@126.com

## REFERENCES

Abramov AV, Aniskin VM, Rozhnov VV. 2012. Karyotypes of two rare rodents, *Hapalomys delacouri* and *Typhlomys cinereus* (Mammalia, Rodentia), from Vietnam. *ZooKeys*, **164**: 41−49.

Abramov AV, Balakirev AE, Rozhnov VV. 2014. An enigmatic pygmy dormouse: molecular and morphological evidence for the species taxonomic status of *Typhlomys chapensis* (Rodentia: Platacanthomyidae). *Zoological Studies*, **53**: 34.

Anjum F, Turni H, Mulder PGH, van der Burg J, Brecht M. 2006. Tactile guidance of prey capture in Etruscan shrews. *Proceedings of the National Academy of Sciences of the United States of America*, **103**(44): 16544−16549.

Baker RJ, Bradley RD. 2006. Speciation in mammals and the genetic species concept. *Journal of Mammalogy*, **87**(4): 643−662.

Bouckaert R, Heled J, Kuhnert D, Vaughan T, Wu CH, Xie D, et al. 2014.

BEAST 2: a software platform for Bayesian evolutionary analysis. *PLoS Computational Biology*, **10**(4): e1003537.

Carmona FD, Jiménez R, Collinson JM. 2008. The molecular basis of defective lens development in the Iberian mole. *BMC Biology*, **6**: 44.

Chen ZZ, He K, Huang C, Wan T, Lin LK, Liu SY, et al. 2017. Integrative systematic analyses of the genus *Chodsigoa* (Mammalia: Eulipotyphla: Soricidae), with descriptions of new species. *Zoological Journal of the Linnean Society*, **180**(3): 694−713.

Cheng F, He K, Chen ZZ, Zhang B, Wan T, Li JT, et al. 2017. Phylogeny and systematic revision of the genus *Typhlomys* (Rodentia, Platacanthomyidae), with description of a new species. *Journal of Mammalogy*, **98**(3): 731−743.

Cheng JL, Lv X, Xia L, Ge DY, Zhang Q, Lu L, et al. 2019. Impact of orogeny and environmental change on genetic divergence and demographic history of *Dipus sagitta* (Dipodoidea, Dipodinae) since the Pliocene in inland East Asia. *Journal of Mammalian Evolution*, **26**(2): 253−266.

Cong HY, Liu ZX, Wang YM, Wang XG, Motokawa M, Harada M, et al. 2013. First record of *Typhlomys cinereus* in Guangdong province. *Acta Theriologica Sinica*, **33**(4): 389−392. (in Chinese)

Cui JF, Lei BY, Newman C, Ji SN, Su HW, Buesching CD, et al. 2020. Functional adaptation rather than ecogeographical rules determine body-size metrics along a thermal cline with elevation in the Chinese pygmy dormouse (*Typhlomys cinereus*). *Journal of Thermal Biology*, **88**: 102510.

Fjeldså J, Bowie RCK, Rahbek C. 2012. The role of mountain ranges in the diversification of birds. *Annual Review of Ecology, Evolution, and Systematics*, **43**: 249−265.

Fu JZ, Zeng XM. 2008. How many species are in the genus *batrachuperus*? A phylogeographical analysis of the stream salamanders (family *hynobiidae*) from southwestern China. *Molecular Ecology*, **17**(6): 1469−1488.

He K, Gutiérrez EE, Heming NM, Koepfli KP, Wan T, He SW, et al. 2019. Cryptic phylogeographic history sheds light on the generation of species diversity in sky-island Mountains. *Journal of Biogeography*, **46**(10): 2232−2247.

Hinckley A, Hawkins MTR, Achmadi AS, Maldonado JE, Leonard JA. 2020. Ancient divergence driven by geographic isolation and ecological adaptation in forest dependent sundaland tree squirrels. *Frontiers in Ecology and Evolution*, **8**: 208.

Hong ZF. 1982. Redescription of *Typhlomys cinereus* Milne-Edward, with a note on its ecology (muscardinidae). *Wuyi Science Journal*, **2**(1): 103−107. (in Chinese)

Jansa SA, Giarla TC, Lim BK. 2009. The phylogenetic position of the Rodent genus *Typhlomys* and the geographic origin of Muroidea. *Journal of Mammalogy*, **90**(5): 1083−1094.

Liu Q, Chen P, He K, Kilpatrick CW, Liu SY, Yu FH, et al. 2012. Phylogeographic Study of *Apodemus ilex* (Rodentia: Muridae) in Southwest China. *PLoS One*, **7**(2): e31453.

Liu XY, Zhang Q, Zhang CL, Yuan FL, Jiao ST. 2017. Global major events in Miocene and its significance: revelation from data mining. *Chinese Science Bulletin*, **62**(15): 1645−1654.

Lv XF, Cong HY, Kong LM, Motokawa M, Harada M, Wu Y, et al. 2016. The nearly complete mitochondrial genome of Chinese pygmy dormouse *Typhlomys cinereus* (Rodentia: Platacanthomyidae). *Mitochondrial DNA*

*Part B*, **1**(1): 605−606.

McCormack JE, Huang H, Knowles LL. 2009. Sky islands. *In*: Gillespie RG, Clague DA. Encyclopedia of Islands. Berkeley: University of California Press, 841-843.

Michaux JR, Chevret P, Filippucci MG, Macholán M. 2002. Phylogeny of the genus *Apodemus* with a special emphasis on the subgenus *Sylvaemus* using the nuclear IRBP gene and two mitochondrial markers: cytochrome *b* and 12S rRNA. *Molecular Phylogenetics and Evolution*, **23**(2): 123−136.

Musser GG, Carleton MD. 2005. Superfamily muroidea. *In* : Wilson DE, Reeder DM. Mammal Species of the World: A Taxonomic and Geographic Reference. Baltimore: Johns Hopkins University Press, 894-1531.

Panyutina AA, Kuznetsov AN, Volodin IA, Abramov AV, Soldatova IB. 2017. A blind climber: the first evidence of ultrasonic echolocation in arboreal mammals. *Integrative Zoology*, **12**(2): 172−184.

Paradis E, Claude J, Strimmer K. 2004. APE: analyses of phylogenetics and evolution in R language. *Bioinformatics*, **20**(2): 289−290.

Riddle BR, Jezkova T, Eckstut ME, Oláh-Hemmings V, Carraway LN. 2014. Cryptic divergence and revised species taxonomy within the Great Basin pocket mouse, *Perognathus parvus* (Peale, 1848), species group. *Journal of Mammalogy*, **95**(1): 9−25.

Ronquist F, Teslenko M, van der Mark P, Ayres DL, Darling A, Hohna S, et al. 2012. MrBayes 3.2: efficient Bayesian phylogenetic inference and model choice across a large model space. *Systematic Biology*, **61**(3): 539−542.

Rubin CT, Lanyon LE. 1984. Dynamic strain similarity in vertebrates; an alternative to allometric limb bone scaling. *Journal of Theoretical Biology*, **107**(2): 321−327.

Smith AT. 2008. Family platacanthomyidae. *In*: Smith AT, Xie Y. A Guide to the Mammals of China. Princeton: Princeton University Press, 208-209.

Song XJ, Tang WQ, Zhang Y. 2017. Freshwater fish fauna and zoogeographical divisions in the Wuyi-Xianxialing Mountains of eastern China. *Biodiversity Science*, **25**(12): 1331−1338. (in Chinese)

Wan T, He K, Jiang XL. 2013. Multilocus phylogeny and cryptic diversity in Asian shrew-like moles (*Uropsilu*s, Talpidae): implications for taxonomy and conservation. *BMC Evolutionary Biology*, **13**: 232.

Wan T, He K, Jin W, Liu SY, Chen ZZ, Zhang B, et al. 2018. Climate niche conservatism and complex topography illuminate the cryptic diversification of Asian shrew-like moles. *Journal of Biogeography*, **45**(10): 2400−2414.

Wang QS. 1990. The Mammal Fauna of Anhui. Heifei: Anhui Publishing House of Science and Technology, 315. (in Chinese)

Wang YX, Li CY, Chen ZP. 1996. Taxonomy, distribution and differentiation on *Typhlomys cinereus* (Platacanthomyidae, Mammalia). *Acta Theriologica Sinica*, **16**(1): 54−66. (in Chinese)

Wu YK, Wang YZ, Jiang K, Hanken J. 2013. Significance of pre-Quaternary climate change for montane species diversity: insights from Asian salamanders (Salamandridae: *Pachytriton*). *Molecular Phylogenetics and Evolution*, **66**(1): 380−390.

Yang ZH, Rannala B. 2010. Bayesian species delimitation using multilocus sequence data. *Proceedings of the National Academy of Sciences of the United States of America*, **107**(20): 9264−9269.

Zhang H, Wu GY, Wu YQ, Yao JF, You S, Wang CC, et al. 2019. A new species of the genus *Crocidura* from China based on molecular and morphological data (Eulipotyphla: Soricidae). *Zoological Systematics*, **44**(4): 279−293.

Zhang JJ, Kapli P, Pavlidis P, Stamatakis A. 2013. A general species delimitation method with applications to phylogenetic placements. *Bioinformatics*, **29**(12): 2869−2876.

Zhou WW, Wen Y, Fu JZ, Xu YB, Jin JQ, Ding L, et al. 2012. Speciation in the *Rana chensinensis* species complex and its relationship to the uplift of the Qinghai-Tibetan Plateau. *Molecular Ecology*, **21**(4): 960−973.